Molecular weight dependence of mobility in polymer blends

Yi Feng* and Charles C. Han†
Polymers Division, National Institute of Standards and Technology, Gaithersburg, MD 20899, USA

Mikihito Takenaka and Takeji Hashimoto
Department of Polymer Chemistry, Kyoto University, Kyoto 606, Japan
(Received 12 August 1991; accepted 30 August 1991)

The molecular weight dependence of mobility in polystyrene/poly(vinyl methyl ether) blends (PS/PVME), in polybutadiene/styrene–butadiene random copolymer (PB/SBR) blends and in polyisoprene/styrene–butadiene random copolymer (PI/SBR) blends has been studied by time resolved light scattering. In the case of PS/PVME, blend samples were quenched from an initial equilibrium temperature, close to the critical temperature, to a final temperature which is deeper in the miscible region. The decay of concentration fluctuations was measured, and the interdiffusion coefficient was deduced, then mobilities were calculated. In the PB/SBR and PI/SBR blends, samples were homogenized by uniaxial compression and interdiffusion coefficients were obtained through time resolved light scattering measurement in the early stage of spinodal decomposition. Mobility was related to the ratio of the interdiffusion coefficient and $q_m^2(0)$, with $q_m(0)$ as the peak position which corresponds to the dominant mode of concentration fluctuations in the early stage of spinodal decomposition. It is clear from our results that mobility can be represented by the vacancy model at lower molecular weights but shows deviation towards the incompressible model at higher molecular weights. The converse can also be said. The overall molecular weight dependence of the mobility can be well represented by the Akcasu–Naegele–Klein equation.

(Keywords: molecular weight dependence; mobility; polymer blends)

INTRODUCTION

The molecular weight dependence of the diffusion process which characterizes the concentration fluctuation or relaxation (interdiffusion) in a binary mixture has been an important and also controversial issue in recent years[1–15]. Theoretically, two limiting cases have been calculated: the first is the incompressible model which was originally calculated by Brochard *et al.*[1] and Binder[2]. This model calculates the interdiffusion of a binary incompressible system, i.e. the total local density is conserved, $\sum \Delta\rho_i = 0$, and therefore the total local flux is also conserved, $J_A + J_B = 0$. The consequence is that the mobility is a weighted inverse sum of the mobilities of individual components. Therefore the slow component controls the mobility of the system and this model has been referred to as the 'slow mode' model.

The second model, the vacancy model, has been proposed by Kramer *et al.*[6] and later by Sillescu[7]. This model assumes that there is an additional vacancy flux besides the fluxes of components A and B, with $J_A + J_B + J_V = 0$ and also $\nabla\mu_v = 0$ (μ_v is the chemical potential for the vacancy). This leads to the so-called 'fast mode' model, in which the mobility is a weighted sum of the mobilities of the individual components. We should point out that both cases are addressing the concentration fluctuation (or relaxation) around the average concentration ϕ_0. In other words, only the first term in the free energy expansion, $(\partial^2 \Delta f/\partial\phi^2)_{\phi_0}$, as well as in the square-gradient expansion, $\nabla^2(\Delta\phi)$ are included. At this level of approximation the (inter)diffusion coefficient can be written as a product of mobility, M, and the second derivative of free energy with respect to the concentration of $\Delta f'' = (\partial^2 \Delta f/\partial\phi^2)_{\phi_0}$ at average concentration ϕ_0. If $\Delta f''$, which is normally molecular weight dependent, can be determined separately then the molecular weight dependence of the mobility, M, at any given concentration and temperature can be determined from the measured experimental results of the interdiffusion coefficient, D_{int}. Thus the question of which (if any) of the two models mentioned above represents the real physical situation can be resolved experimentally.

In order for any experimental test to be conclusive, several conditions have to be met. (1) The non-linear contribution from the higher order terms of both the free energy expansion and the gradient expansion to the diffusion process has to be avoided. Therefore, the experiment has to be carried out or extrapolated to a concentration condition such that either the concentration gradient or the concentration difference between the two

* Permanent address: Department of Polymer Science and Engineering, East China University of Chemical Technology, Shanghai, 200237, P.R. China
† To whom correspondence should be addressed

0032-3861/92/132729-11

testing layers approaches zero ($\phi_2 - \phi_1 \sim 0$). (2) A wide range is needed in the molecular weight dependence study in order to distinguish these two models. (3) $\Delta f'' = (\partial^2 \Delta f/\partial \phi^2)_{\phi_0}$ or a quantity proportional to $\Delta f''$ needs to be determined separately in order to extract the mobility M, and then to examine the molecular weight dependence of M. (4) All data have to be either measured or reduced to the same T and ϕ. This is because both M and $\Delta f''$ could be strong functions of T and ϕ; the comparison of the molecular weight dependence of M is only meaningful if M values can be obtained at the same T and ϕ.

In this paper we will present studies on three separate systems: polystyrene/poly(vinyl methyl ether) (PS/PVME) system; polybutadiene/styrene–butadiene random copolymer (PB/SBR) system; and polyisoprene/styrene–butadiene random copolymer (PI/SBR) system.

In the study of PS/PVME we used the temperature jump (or quench) method and time resolved light scattering to measure D_{int} at various temperatures with four different PS samples. The experiment was actually carried out by quenching the sample in the single phase state from a temperature which is close to the critical point to another temperature which is away from critical temperature. We then measured the time dependence of the decrease of concentration fluctuation from one equilibrium state to another by measuring the time resolved static structure factor, $S(q, t)$. Since we were measuring changes of equilibrium concentration fluctuations as we varied temperature, the results can be analysed by the linearized diffusion equation without having to carry out further concentration extrapolations to minimize the contribution from higher order terms in the free energy and concentration gradient expansion[2,16–19]. We then obtain the temperature dependence of the mobility from

$$M(T) = D_{\text{int}}(T)/\Delta f''(T)$$

by using the separately determined value of $\Delta f''(T)$. Finally we can compare the molecular weight dependence of M at any given temperature.

In the study of PB/SBR and PI/SBR systems, blend samples were homogenized by a uniaxial compression method[20–22] and then the early stage of spinodal decomposition was studied by the time resolved light scattering technique. Data were analysed according to the Cahn–Hilliard theory[16,17] and the interdiffusion coefficients were obtained. Since these two systems are immiscible within the experimentally accessible temperature range, it is impossible to measure the free energy of mixing or its derivatives directly. However, the wave number $q_m(0)$ for the dominant mode of the concentration fluctuations in the early stage of spinodal decomposition has been measured, which is related to $\Delta f''$. Therefore the relative mobilities for different molecular weights can be obtained and compared.

THEORETICAL BACKGROUND

The time evolution of the scattering structure factor due to concentration fluctuations in a binary mixture in the early stage of spinodal decomposition can be represented by the linearized model of Cahn–Hilliard–Cook[2,16,17]. Actually this linearized theory represents well the kinetic process of a system with a reverse quench from near critical temperature (or a system just into the spinodal region for a short time) which has a large concentration fluctuation back to a temperature deep into the miscible region. This linearized diffusion equation can be written as:

$$\frac{\partial S(q,t)}{\partial t} = -2Mq^2\left[\left(\frac{\partial^2 \Delta f}{\partial \phi_0^2} + 2\kappa q^2\right)S(q,t)\right] + 2Mk_B T q^2 \tag{1}$$

where M is the mobility defined as the proportionality constant in the relation between interdiffusion current density and chemical potential gradient; q is the magnitude of the scattering wave vector ($=(4\pi n/\lambda)\sin\theta/2$, with n the refractive index and θ the scattering angle); Δf is the free energy density for a uniform system; ϕ_0 is the average composition; κ is an interfacial free energy coefficient defined as the proportionality constant in relation between interfacial free energy density and the square of concentration gradient; k_B is the Boltzmann constant.

The solution for the linearized diffusion equation (equation (1)) can be obtained as:

$$S(q,t) = S_\infty + (S_0 - S_\infty)\, e^{2R(q)t} \tag{2}$$

where S_∞ is the so-called 'virtual structure factor' arising from the thermal noise term $2Mk_BTq^2$, and S_0 is structure factor[19] at $t = 0$. The growth rate $R(q)$ is given as:

$$R(q) = -Mq^2[\partial^2 \Delta f/\partial \phi_0^2 + 2\kappa q^2] \tag{3}$$

In the unstable (spinodal) region $(\partial^2 \Delta f/\partial \phi^2)_{\phi_0}$ is negative, which gives positive $R(q)$ at small q or large wavelength of concentration fluctuation growth. On the other hand, in the case of reverse quench (into the miscible region), the change of the structure factor associated with concentration fluctuation decay is also governed by equations (2) and (3). In this case, $R(q)$ is a negative quantity referred to as a decay rate. This is because $\partial^2 \Delta f/\partial \phi_0^2$ is positive in the stable region.

Equation (3) can be rewritten as:

$$R(q) = -D_{\text{int}}q^2 - 2M\kappa q^4 \tag{4}$$

with the interdiffusion coefficient:

$$D_{\text{int}} = M\,\partial^2 \Delta f/\partial \phi_0^2 \tag{4'}$$

By taking the limit as $t \to \infty$ in equation (1)[2,19], the rate of growth (or decay) can be written as:

$$R(q) = -\frac{Mk_BT}{S(q)_T}q^2 \tag{5}$$

with $S(q)_T$ replacing the virtual structure factor S_∞ in the case where the final temperature is in the unstable region. However, $S(q)_T$ is the thermal equilibrium structure factor at the final temperature in the case where the final state is in the stable (or miscible) region. This structure factor for a binary polymer system has been calculated with random phase approximation by deGennes[23,24], Binder[2] and others as:

$$S(q)_T^{-1} = \frac{1}{N_A\phi_A v_A S_A(q)} + \frac{1}{N_B\phi_B v_B S_B(q)} - \frac{2\chi}{v_0} \tag{6}$$

where N_i is the degree of polymerization; ϕ_i is the volume fraction of component i; v_i is the segmental volume of component i; $S_i(q)$ is the Debye function of component i; χ is the pair interaction parameter per segment. In the zero wave number or thermodynamic limit ($q \to 0$),

$S_i(q) = 1$ and equation (6) becomes:

$$S(q \to 0)^{-1} = \frac{\partial^2(\Delta f/k_B T)}{\partial^2 \phi_0} = \frac{1}{N_A \phi_A v_A} + \frac{1}{N_B \phi_B v_B} - \frac{2\chi}{v_0}$$

$$\equiv \frac{2}{v_0}(\chi_s - \chi) \qquad (7)$$

Actually equation (7) can be obtained easily by combining equations (3), (5) and (6). By combining experimentally obtained $\partial^2 \Delta f/\partial \phi_0^2$ and D_{int}, the molecular weight dependence of the mobility can be obtained from equation (4') at various temperatures and compositions. In cases where $\partial^2 \Delta f/\partial \phi_0^2$ cannot be measured directly (such as the PB/SBR and PI/SBR systems reported in this paper), the relative mobility can still be calculated if the early stage spinodal decomposition kinetics can be obtained. From equation (3) it can be easily shown that the maximum growth rate happens at:

$$q^2 = q_m^2(0) = -\Delta f''/4\kappa \qquad (8)$$

From equations (3), (5) and (6) it can be shown that:

$$\kappa = \frac{k_B T}{36}\left(\frac{b_A^2}{\phi_A v_A} + \frac{b_B^2}{\phi_B v_B}\right)$$

$$\equiv \frac{k_B T v_0 b^2}{36 \phi_A \phi_B v_A v_B} \qquad (9)$$

with $v_0 b^2 \equiv \phi_B v_B b_A^2 + \phi_A v_A b_B^2$, and b_i is the statistical segment length of the ith polymer. Then from equations (8), (9) and (4'), it is clear that:

$$D_{int}/q_m^2(0) = M\,\Delta f''/(-\Delta f''/4\kappa)$$

$$= -\frac{M b^2 k_B T v_0}{9 \phi_A \phi_B v_A v_B} \equiv M' \qquad (10)$$

In order to make comparison with the incompressible (or slow mode) model by deGennes, Brochard *et al.*[1] and Binder[2], or the vacancy (or fast mode) model by Kramer[6] and Sillescu[7,8], we will also write down their results with proper constants to facilitate comparison with our experimental results.

The D_{int} from the vacancy (fast mode) calculation can be written as:

$$D_{int} = [(1 - \phi_A)N_A D_A + \phi_A N_B D_B] \times \left(\frac{\phi_A(1 - \phi_A)v_0}{k_B T}\right)\left(\frac{\partial^2 \Delta f}{\partial \phi_A^2}\right) \qquad (11)$$

where D_i is the tracer diffusion coefficient of component i in the A/B blend of composition ϕ_i. In the bulk entangled case, the tracer diffusion coefficient of a polymer chain will follow an inverse molecular weight square dependence. Therefore, D_i can be written as:

$$D_i = D_1^i N_i^{-2} \qquad (12)$$

where N_i is the degree of polymerization of the ith component; and D_1^i is the diffusion coefficient of monomer i.

The mobility for the vacancy model can be written from equations (4), (11) and (12) as:

$$M = \frac{\phi_A(1 - \phi_A)v_0}{k_B T}[(1 - \phi_A)N_A D_A + \phi_A N_B D_B] \qquad (13)$$

$$= \frac{\phi_A(1 - \phi_A)v_0}{k_B T}\left[\frac{(1 - \phi_A)D_1^A}{N_A} + \frac{\phi_A D_1^B}{N_B}\right] \qquad (13')$$

Similarly, the mobility for the incompressible model can be written as:

$$\frac{1}{M} = \frac{k_B T}{\phi_A(1 - \phi_A)v_0}\left[\frac{(1 - \phi_A)}{D_A N_A} + \frac{\phi_A}{D_B N_B}\right] \qquad (14)$$

$$= \frac{k_B T}{\phi_A(1 - \phi_A)v_0}\left[\frac{(1 - \phi_A)N_A}{D_1^A} + \frac{\phi_A N_B}{D_1^B}\right] \qquad (14')$$

EXPERIMENTAL

Samples

As shown in *Table 1*, all PS samples used in this study are standard samples with a narrow molecular weight distribution. The PVME was cationically polymerized and fractionated in toluene/n-heptane. The molecular weight and polydispersity of PVME were determined by g.p.c.[25].

All PS/PVME samples were made of 80 wt% PVME and 20 wt% PS, and contain 0.05 wt% of 4,4'-thiobis-(6,tert-butyl-m-cresol) as the antioxidant. Specimens were prepared by casting from toluene solutions (~10% total polymer concentration) on quartz window plates. The solvent-cast film was dried in vacuum at room temperature for 2 days, then at 70°C for 2 days and was then covered by another quartz plate with a metal spacer to maintain specimen thickness and annealed at 60°C overnight. The thickness of the specimen used for spinodal decomposition was 0.1 mm, while that for studying the decay of concentration fluctuation was 0.2 mm.

All PB/SBR and PI/SBR samples were made by the same procedure as described before[20–22]. Molecular weights and polydispersities of all SBR, PB and PI samples are listed in *Table 2*.

Table 1 Molecular weight and polydispersity of PVME and PS samples

Sample	M_w	M_w/M_n
PS1 (TSK standard)	1.86×10^5	1.07
PS2 (TSK standard)	3.55×10^5	1.02
PS3 (NIST standard)	1.05×10^6	<1.1
PS4 (Pressure chemical standard)	2×10^6	<1.2
PVME	2×10^5	1.42

Table 2 Molecular weight and polydispersity of SBR, PB and PI samples

Sample	M_w	M_w/M_n	Styrene (wt%)
SBR1	1.18×10^5	1.18	20
SBR10	8.3×10^4	1.2	20
PB5	4.9×10^4	1.4	–
PB10	8.9×10^4	1.6	–
PB20	2.23×10^5	1.3	–
PB100	1.03×10^6	2.4	–
PI20	2.05×10^5	1.3	–
PI55	5.46×10^5	1.1	–
PI122	1.22×10^6	1.3	–
PI273	2.73×10^6	1.5	–

Measurement

The temperature jump light scattering measurements for PS/PVME blends were carried out at NIST on a time-resolved static light scattering instrument[19], which uses a 5 MW He-Ne laser as the incident beam and a set of neutral density filters to keep the scattering intensity within the dynamic range of the one-dimensional photodiode array detector (Radicon tube). The sensitivity of the detector array was calibrated by fluorescence radiation from nile blue dye (5×10^{-6} g ml^{-1}) embedded in gelatin gel in the same cell as used in blend measurements. An optical multichannel analyser (OMA3)* was used for data acquisition. The collection, collimation and angular mapping of scattering light were accomplished by a set of lens systems.

The temperature jump was carried out by quickly transferring samples from the pre-heating block to the main block. The preheating block was used to anneal the sample at a temperature in the miscible region in order to bring the sample to a completely relaxed state. The main block was controlled at a desired experimental temperature. Both blocks are controlled by PID controllers to within ± 0.02°C of the specified temperature. The sample was kept in the preheating block for about 2 h before measurement. It takes about 1 min to reach temperature equilibrium (with a time constant of about 20 s) after transferring the sample from the preheating block to the main block. Therefore, the initial time of the experiment was chosen to be 1 min after transferring the sample.

For the PB/SBR and PI/SBR blends, the time-resolved static light scattering experiments were carried out in Kyoto University, Japan. The detailed instrumentation and procedure have been described elsewhere[20–22].

RESULTS AND DISCUSSION

For the PS/PVME system, two sets of temperature jump and time resolved light scattering experiments were carried out for each molecular weight combination. One set is to jump from the miscible region to the unstable (spinodal) region in order to study the q-dependent growth rate, $R(q)$, in the early stage of spinodal decomposition as a function of final temperature. The second set of experiments is a set of reverse quench experiments performed by changing temperature from close to phase separation to far into the miscible region with various final temperatures. Of course, fresh samples have to be prepared each time, especially in the first set of experiments. A typical set of intensity growth data as a function of time for various scattering wave vectors, q, after jump into the spinodal region are displayed in *Figure 1* for PS1 ($M_w = 1.86 \times 10^5$). The corresponding 1/3-power plots are displayed in *Figure 2*. As explained in a previous paper[19], the initial slope divided by the intercept yields $R(q)/3$ in this plot. The corresponding Cahn plots, which are $R(q)/q^2$ *versus* q^2 plots, are shown in *Figure 3*. According to equation (4) the intercept of this plot is the interdiffusion coefficient, D_{int}. The main purpose of carrying out this set of experiments is to locate the spinodal temperature as a function of molecular weight for each of the four samples. Later on we will use these data to obtain corresponding values for $\partial^2 \Delta f/\partial \phi_0^2$.

In the second set of experiments, the blend sample was annealed at a temperature slightly below its spinodal temperature, which was obtained from the first set of measurements. Then the sample was quenched down to

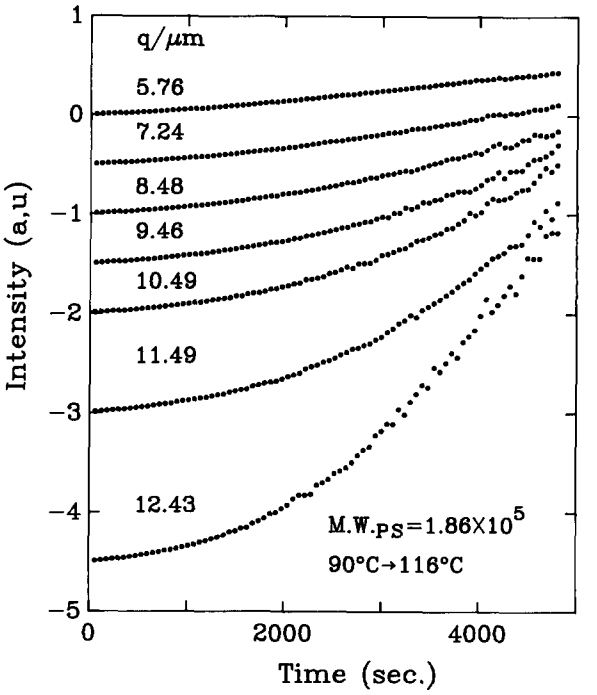

Figure 1 Scattering intensities at various scattering wave vectors, q, are plotted as a function of time after the temperature of the specimen has been jumped from 90 to 116°C. The specimen is a PS/PVME blend with 20 wt% PS ($M_w = 1.86 \times 10^5$). Curves are shifted vertically to avoid overlapping

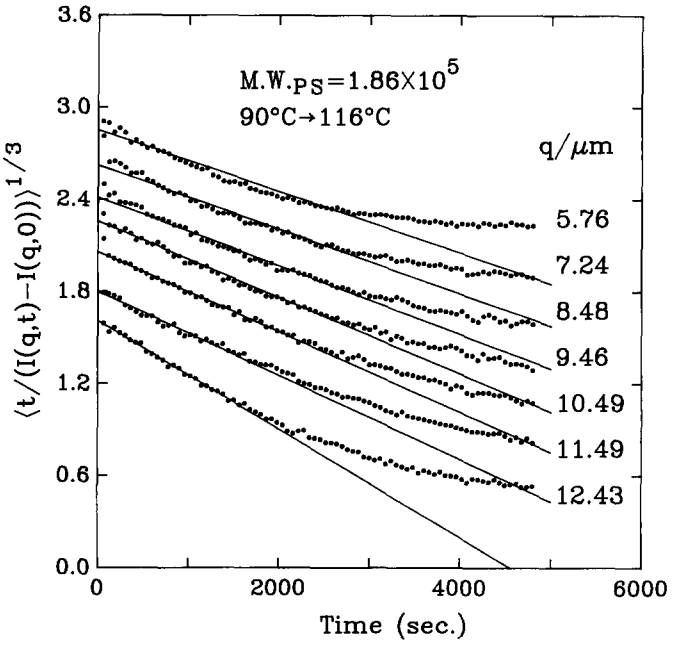

Figure 2 The scattering intensity obtained as in *Figure 1* is plotted as $\{t/[I(q,t) - I(q,0)]\}^{1/3}$ *versus* time. The slope of this plot gives the q-dependent growth rate, $R(q)$. Curves are shifted vertically to avoid overlapping; the $q = 5.76\ \mu m^{-1}$ curve is not shifted but every other curve is shifted down by an additional 0.1 start from the $q = 7.24\ \mu m^{-1}$ curve

In the second set of experiments, the blend sample was annealed at a temperature slightly below its spinodal temperature, which was obtained from the first set of measurements. Then the sample was quenched down to

* Certain commercial materials and equipment are identified in this paper in order to specify adequately the experimental procedure. In no case does such identification imply recommendation or endorsement by the National Institute of Science and Technology, nor does it necessarily imply the best available for the purpose

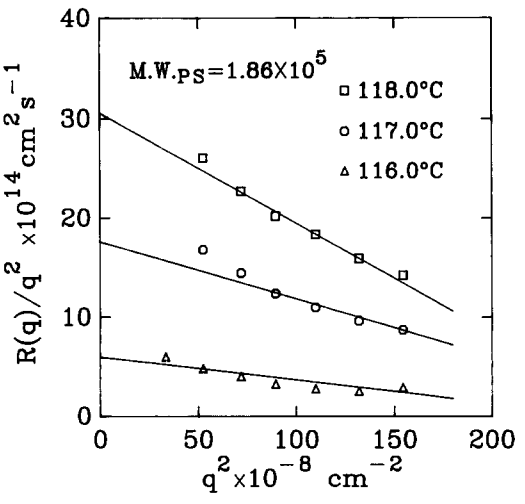

Figure 3 The growth rate for different jump depths obtained in plots such as *Figure 2* for sample 1 is plotted as $R(q)/q^2$ *versus* q^2. The intercept of the straight line fit gives D_{int} according to equation (4)

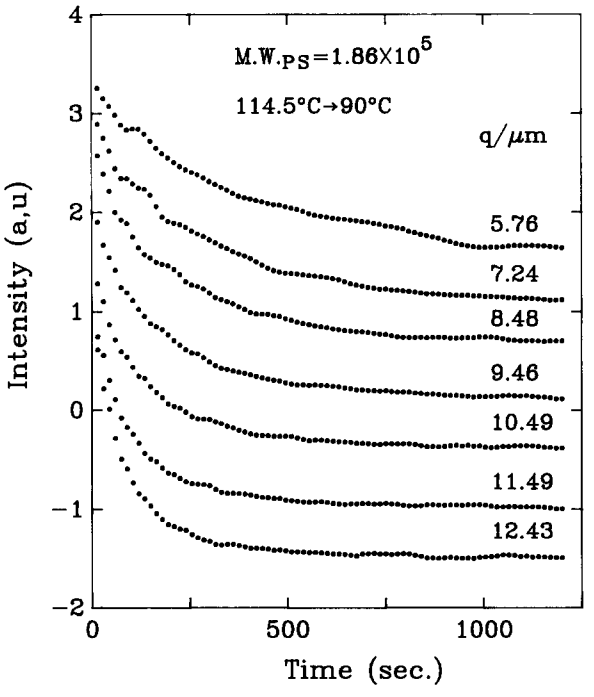

Figure 4 Scattering intensities for PS/PVME sample 1, after quench from 114.5 to 90°C, are plotted as a function of time for various q values. Curves are shifted vertically to avoid overlapping

various temperatures in the miscible region. The purpose of this choice is to have a large enough change of scattering structure factor after the temperature quench. Meanwhile, both initial and final states are well defined equilibrium states whose concentration fluctuations are not too large; therefore, the non-linear effects caused particularly by the large concentration gradient can be neglected.

Typical scattering intensity (which is proportional to the structure factor $S(q)$) decay curves after a temperature quench from 114.5 to 90°C are displayed in *Figure 4* for the PS1 ($M_w = 1.86 \times 10^5$) sample at various q values. The slope of the semilogarithmic plot of $[I(q,t) - I(q,t=\infty)]$ *versus* time equals $2R(q)$ according to equation (2). These are displayed in *Figure 5* for the data set obtained from *Figure 4*. In *Figure 6*, $-R(q)$ is plotted against q^2 to demonstrate the q^2 dependence of $R(q)$. Also, the fitted straight lines which all pass through the origin are good indications that the rate of decay of concentration fluctuations can be represented by equation (2) with negligible contributions from interfacial free energy. In *Table 3*, D_{int} results are given for all four PS samples in the spinodal region obtained with the procedure illustrated above. Since PS/PVME blends all have lower critical solution temperatures the temperature 'jump' experiments (into the spinodal region) are characterized by a negative D_{int} which indicates growth

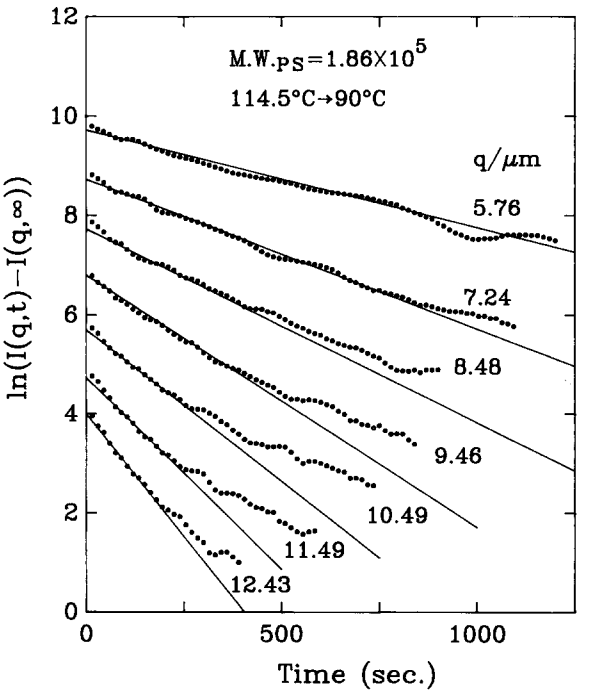

Figure 5 Semilogarithmic plot of $[I(q,t) - I(q,t=\infty)]$ as a function of time for PS/PVME sample 1. The slope of this plot gives the decay rate, $R(q)$, according to equation (2). Curves are shifted vertically to avoid overlapping

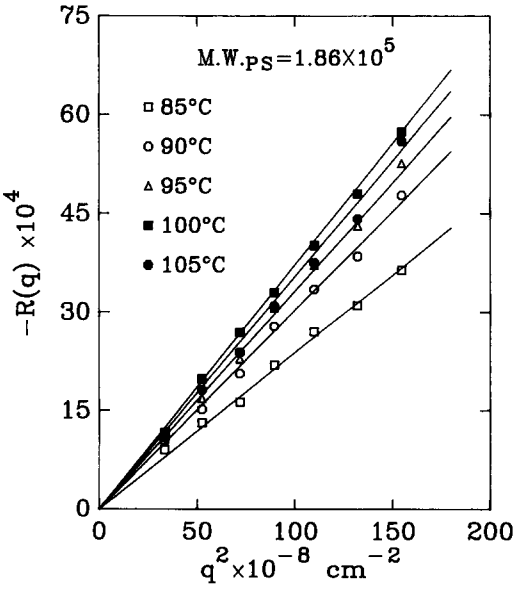

Figure 6 The negative decay rates, $-R(q)$, obtained from plots similar to *Figure 5* are plotted as a function of q^2 for various quench depths as indicated in the figure. The solid lines are best fitted straight lines through the origin. The slope of this line gives D_{int}

in fluctuation size. On the contrary, all temperature 'quench' experiments (within the miscible region) are characterized by a positive D_{int} which indicates decay in fluctuation size. Results of D_{int} in this miscible region are listed in *Table 4*. In *Figure 7*, D_{int} is plotted against temperature for all four sets of molecular weights. Smooth curves are drawn through the experimental data. The curves are shifted up 5°, 3° and 2°C for PS1 ($M_w = 1.86 \times 10^5$), PS2 ($M_w = 3.55 \times 10^5$) and PS3 ($M_w = 1.05 \times 10^6$) data sets, respectively, to avoid overlapping. The spinodal temperature, T_s, is characterized by $D_{int} = 0$ because $(\partial^2 \Delta f/\partial \phi_0^2)_{T_s} = 0$ at spinodal temperature. The spinodal temperatures obtained by extrapolating D_{int} data obtained in the unstable region to $D_{int} = 0$ are also listed in *Table 3*. These spinodal temperatures are used in the second set of experiments (quench experiments) to help determine the initial temperature which is selected to be less than 2°C lower than its corresponding T_s. These spinodal temperatures are also used to calculate the corresponding values of $\partial^2 \Delta f/\partial \phi_0^2$ which will be used later. It has been shown in a previous paper[19] that the $\partial^2 \Delta f/\partial \phi^2$ values can be represented by:

$$\frac{\partial^2 \Delta f}{\partial \phi^2} = 2.18 \times 10^3 (1/T - 1/T_s)\ \mathrm{J\ cm^{-3}} \quad (15)$$

for a deuterated polystyrene (PSD)/PVME system with 20% PS and 80% PVME. Although hydrogenated polystyrene (PSH) is being used in this study, there is no reason to believe that the temperature dependence of $\partial^2 \Delta f/\partial \phi^2$ will be very different from deuterated PS. Actually, recent SANS work[26] of a three-component PSD/PSH/PVME system has indicated that the

Table 3 D_{int} for the PS/PVME blends in the early stage of spinodal decomposition

Sample	Initial temp. (°C)	Final temp. (°C)	$-D_{int} \times 10^{14}$ ($cm^2\ s^{-1}$)	T_s (°C)
PS1		116	6.0	
($M_w = 1.86 \times 10^5$)	90	117	17.6	115.2
		118	30.6	
PS2		115.5	6.5	
($M_w = 3.55 \times 10^5$)	90	116.0	10.0	114.3
		116.5	13.5	
PS3		111.5	0.8	
($M_w = 1.06 \times 10^6$)	90	112.5	4.8	111.2
		113.5	10.0	
		114.0	13.5	
PS4		110	0.4	
($M_w = 2 \times 10^6$)	90	111	1.5	109.6
		112	2.5	

Table 4 D_{int} for the PS/PVME blends in one phase reverse temperature quench

Sample	Initial temp. (°C)	Final temp. (°C)	$D_{int} \times 10^{14}$ ($cm^2\ s^{-1}$)
PS1		85	23.8 ± 0.7
($M_w = 1.86 \times 10^5$)		90	30.2 ± 0.9
	114.5	95	33.1 ± 1.0
		100	37.1 ± 1.1
		105	35.3 ± 1.1
PS2		85	17.3 ± 0.5
($M_w = 3.55 \times 10^5$)		90	19.1 × 0.6
	112	95	23.9 ± 0.7
		100	26.6 ± 0.8
		105	20.9 ± 0.6
PS3		85	12.0 ± 0.4
($M_w = 1.06 \times 10^6$)	109	90	13.7 ± 0.4
		100	16.1 ± 0.5
		105	15.0 ± 0.5
PS4		85	7.5 ± 0.3
($M_w = 2 \times 10^6$)	108	90	8.3 ± 0.3
		95	9.3 ± 0.3
		100	8.8 ± 0.3

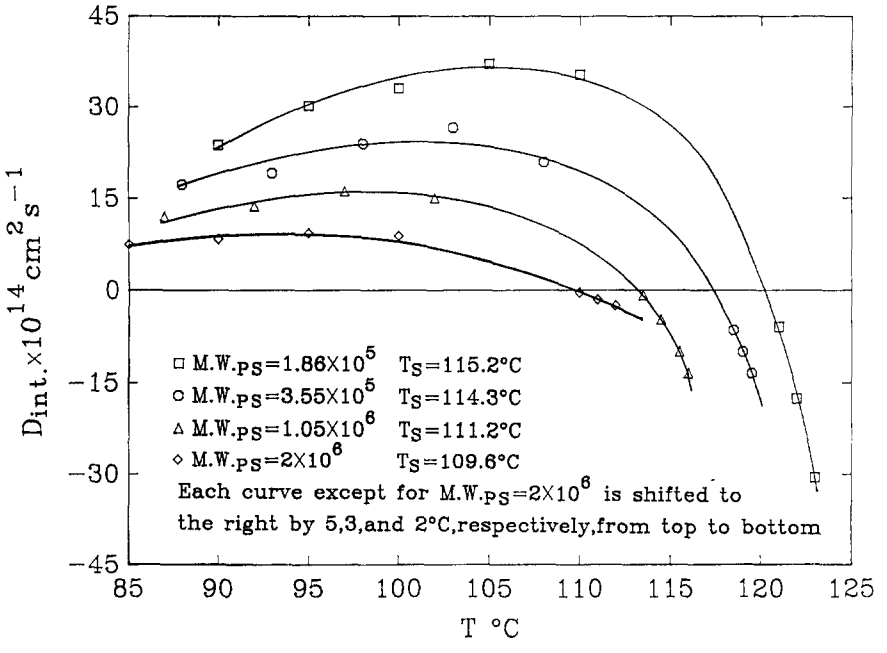

Figure 7 The interdiffusion coefficient, D_{int}, for both jump and quench cases for all four PS/PVME samples are displayed as a function of temperature. Smooth curves are drawn through data points. The extrapolated temperatures at $D_{int} = 0$ are the spinodal temperatures of the corresponding blend samples. Notice that the temperatures are shifted by 5°C, 3°C and 2°C to the right for samples PS1, PS2 and PS3, respectively, to avoid overlapping

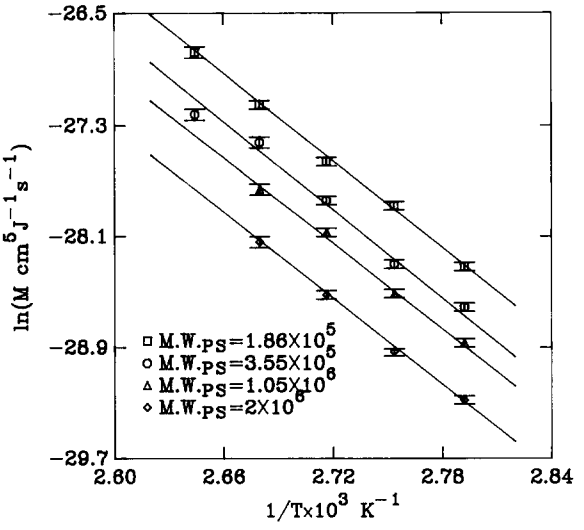

Figure 8 Logarithm of mobilities of PS/PVME obtained from *Figure 7* and equations (4′) and (15) are plotted against $1/T$. The solid lines are best fit straight lines

temperature dependence of $\partial^2 \Delta f/\partial\phi^2$ for PSH/PVME is very much the same as that of PSD/PVME blends; we have therefore used equation (15) in the reduction of our D_{int} data into mobility, M.

In *Figure 8*, the logarithm of mobility is plotted against $1/T$ for all four sets of molecular weights. It can be seen that the temperature dependence of M for all four molecular weights follows an Arrhenius behaviour in this temperature range and that the slopes are equal. The activation energy is about 20 kcal mol^{-1}. The straight lines are a best linear fit to each data set. In order to examine the molecular weight dependence, we arbitrarily selected two temperatures, 103°C ($1/T = 0.00266$ K^{-1}) and 84°C ($1/T = 0.0028$ K^{-1}), and interpolated M values for all four PS molecular weight sets from the straight line fit in *Figure 8*. The results are plotted as M *versus* $1/N_{PS}$ and $1/M$ *versus* N_{PS} in *Figure 9a* and *b*, respectively. According to the vacancy model (equation (13′)) *Figure 9a* should give straight lines for all mobility data. It seems that low molecular weight data can be represented by straight lines very well, but at the largest molecular weight, M definitely shows deviation. On the other hand, if the incompressible or slow mode model (equation (14′)) is correct then the $1/M$ *versus* N_{PS} plot (*Figure 9b*) should be a straight line. Again we see deviation from a straight line, but this time the deviation is in the smallest molecular weight data. We also sketched dotted curves to go through all data points without attaching any special significance, except that the arrows at intercepts are calculated from the solid line intercept of the other model plots. For example the intercept, I_f, of equation (13′) should be

$$I_f = \phi_A(1-\phi_A)v_0/k_BT(\phi_A D_1^B/N_B)$$

while the intercept, I_s, from equation (14′) is

$$I_s = k_BT/[\phi_A(1-\phi_A)v_0](\phi_A N_B/D_1^B)$$

The product is

$$I_f I_s = \frac{\phi_A(1-\phi_A)v_0}{k_BT}\left(\frac{\phi_A D_1^B}{N_B}\right)\frac{k_BT}{\phi_A(1-\phi_A)v_0}\left(\frac{\phi_A N_B}{D_1^B}\right)$$
$$= \phi_A^2 \qquad (16)$$

Therefore from *Figure 9a*, the straight line intercept obtained from the fast mode analysis can be used to predict the corresponding intercept in the slow mode plot in *Figure 9b*. These are shown by arrows in *Figure 9b*. Conversely, the solid line intercepts obtained from the slow mode plot in *Figure 9b* can be used to predict their corresponding intercepts in the fast mode plot in *Figure 9a*, also indicated by arrows. From the dashed lines in *Figure 9a* and *b*, it does seem that data tend to follow slow mode behaviour in the large molecular weight range and tend towards fast mode behaviour in the smaller

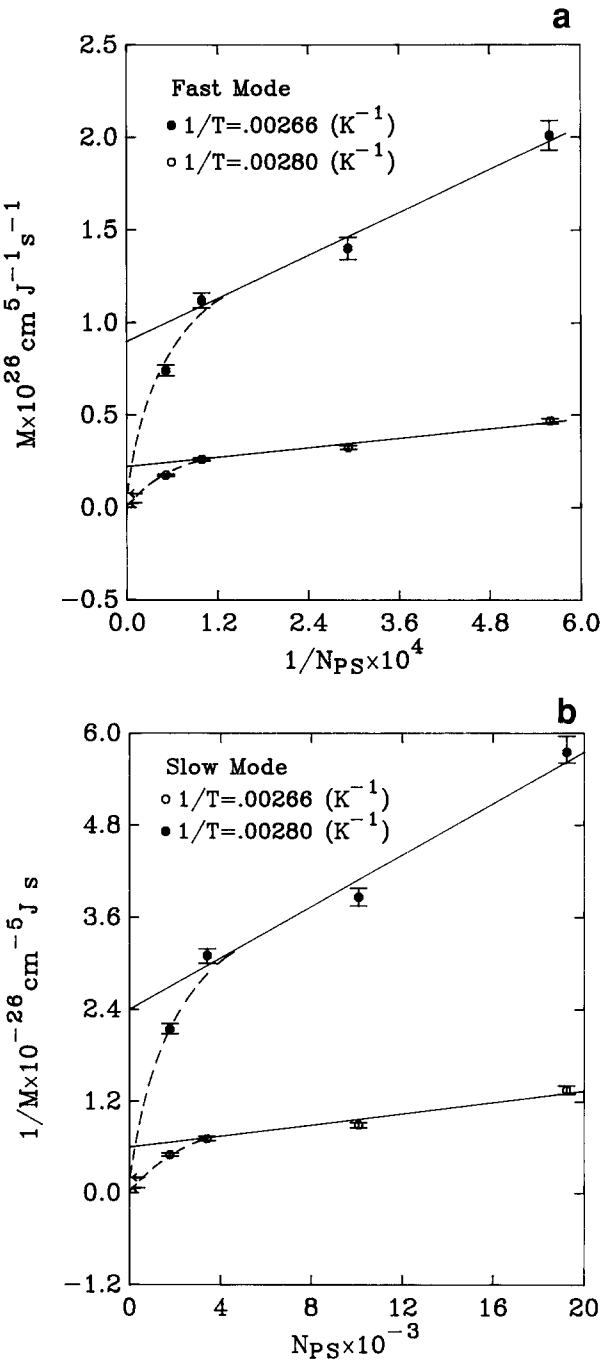

Figure 9 Mobilities at 103°C ($1/T = 0.00266$ K^{-1}) and 84°C ($1/T = 0.0028$ K^{-1}) interpolated from *Figure 8*. (a) M *versus* inverse of degree of polymerization of PS, $1/N_{PS}$: solid lines are best fit straight lines for the three low M_w data points; dashed lines are hand drawn lines through data points; arrows at intercepts are obtained from *Figure 9b*. (b) $1/M$ *versus* N_{PS}: solid lines are best fit straight lines for the three large N_{PS} data points; dashed lines are hand drawn through low M_w data (conversely to *Figure 9a*); the two arrows are obtained from the straight line intercepts of *Figure 9a*

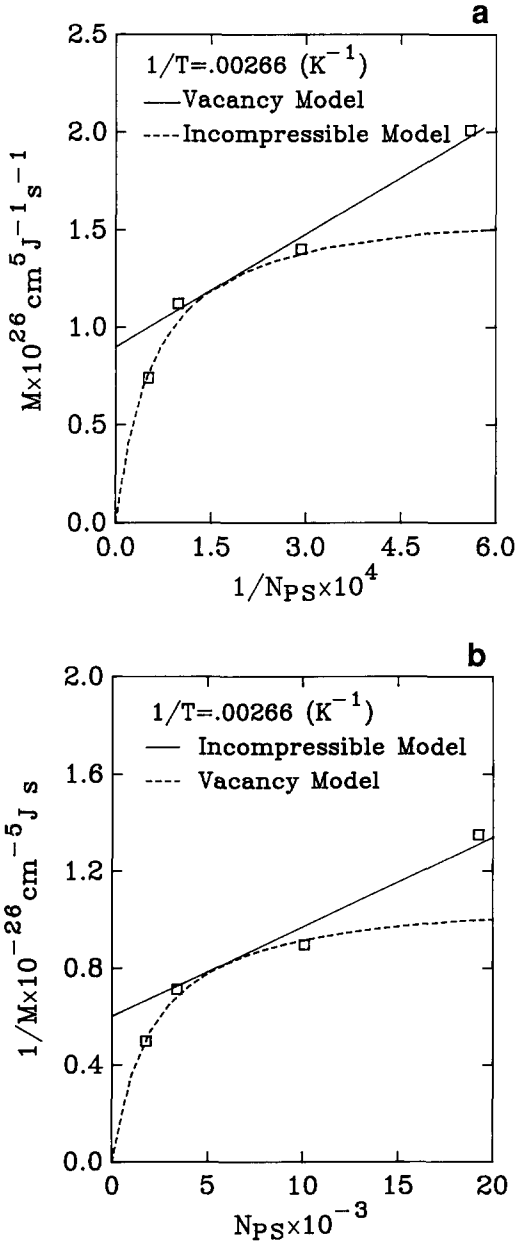

Figure 10 (a) Mobility data, M *versus* $1/N_{PS}$ for PS/PVME are displayed (for $1/T = 0.00266$) together with a straight line fit of the fast mode model through three low M_w data points and the dashed line for slow mode through high M_w data. (b) Inverse of mobility data, $1/M$ *versus* N_{PS} are displayed, together with a straight line fit of slow mode model through high M_w data and a dashed line for fast mode model through low M_w data

molecular weight range. This can be seen more clearly by plotting the corresponding straight line values on the inverse plot. For example, M *versus* $1/N_{PS}$ is plotted in *Figure 10a* for $1/T = 0.00266\ K^{-1}$ together with a dotted line which uses the same slope and intercept values obtained from the solid line from *Figure 10b*. A similar plot for $1/M$ *versus* N_{PS} is also made in *Figure 10b*.

From *Figures 9a, b* and *10a, b*, it seems that the mobility data can be represented by either the vacancy or the incompressible model equally well (or badly). The vacancy model is more consistent with lower molecular weight data, with some deviation at high molecular weights. On the other hand, the incompressible model is more consistent with high molecular weight data, with some deviations at low molecular weights. The question is, does either of these two model functions represent the real physical situation for the whole molecular weight range?

Recently, the interdiffusion coefficient for an incompressible ternary system has been calculated using a three-component dynamic random phase approximation approach[27–29]. In this calculation, the third component can be treated as vacancies and one then recovers both the 'fast mode' and the 'slow mode' theories as limiting cases when the product of the mole fraction and the corresponding monomer diffusion coefficient, $X = \phi_c D_1^c$ approaches infinity or zero, respectively. For entangled cases ($D \sim 1/N^2$), the Akcasu–Naegele–Klein (ANK) equation can be written as follows:

$$M = \frac{\phi_A^2\phi_B^2 v_0}{k_B T}\left[\frac{D_1^A}{\phi_A N_A} + \frac{D_1^B}{\phi_B N_B} - \frac{\left(\frac{D_1^A}{N_A} - \frac{D_1^B}{N_B}\right)^2}{\phi_A \frac{D_1^A}{N_A} + \phi_B \frac{D_1^B}{N_B} + \phi_c D_1^c}\right] \tag{17}$$

$$= \frac{\phi_A^2\phi_B^2 v_0 D_1^B}{k_B T}\left[\frac{\alpha}{\phi_A N_A} + \frac{1}{\phi_B N_B} - \frac{\left(\frac{\alpha}{N_A} - \frac{1}{N_B}\right)^2}{\frac{\phi_A \alpha}{N_A} + \frac{\phi_B}{N_B} + X'}\right] \tag{17'}$$

with $\alpha = D_1^A/D_1^B$ and $X' = \phi_c D_1^c/D_1^B$. By using this ANK equation, our mobility data can be represented as in *Figures 11a* and *b*. In *Figure 11a*, we have used values of $\phi_A = 0.2$, $\phi_B = 0.8$, $v_0 = 1.66 \times 10^{-22}\ cm^3$, $\alpha = 0.3$, $X' = 0.0005$ and $D_1^B = D_1^{PVME} = 4.4 \times 10^{-7}$ (at $1/T = 0.0028\ K^{-1}$) and $2 \times 10^{-6}\ cm^2\ s^{-1}$ (at $1/T = 0.00266\ K^{-1}$). The same data sets and curves can be replotted in the inverse version shown in *Figure 11b*. It is clear that all data can be represented very nicely by the ANK equation. Furthermore, the ratio of the two D_1^{PVME} values used in the two corresponding fittings is 4.5, which is very close to the ratio of mobilities of 4.2, calculated from *Figure 8* for the same two temperatures. This implies that, within this temperature range, the assumption that α and X' in equation (17') are temperature-independent quantities does not cause any inconsistency in this analysis. For the SBR/PB and the SBR/PI systems, as mentioned earlier, we were unable to obtain the $\Delta f''$ directly. However, in the time resolved light scattering study of the early stage of spinodal decomposition, the wave number $q_m(0)$ for the dominant mode of the concentration fluctuations and the value D_{int} were determined from the Cahn plot shown in *Figure 3*, and the relative mobility can be obtained by dividing D_{int} by $q_m^2(0)$ according to equation (10). In *Table 5* the experimental temperature, the interdiffusion coefficient D_{int}, which was obtained with a similar procedure used for the PS/PVME blends described above, and the peak position, $q_m(0)$, at an early stage of spinodal decomposition for all eight blends are listed. We analysed these results of the relative mobility, M', from these two sets of SBR blends by the same procedure used above for the PS/PVME blends. In *Figure 12a*, the relative mobility M' for SBR10/PB blends is plotted against the inverse of the degree of polymerization of PB, while in *Figure 12b*, $1/M'$ *versus* N_{PB} is displayed. The circles represent experimental data. As in the case of PS/PVME systems,

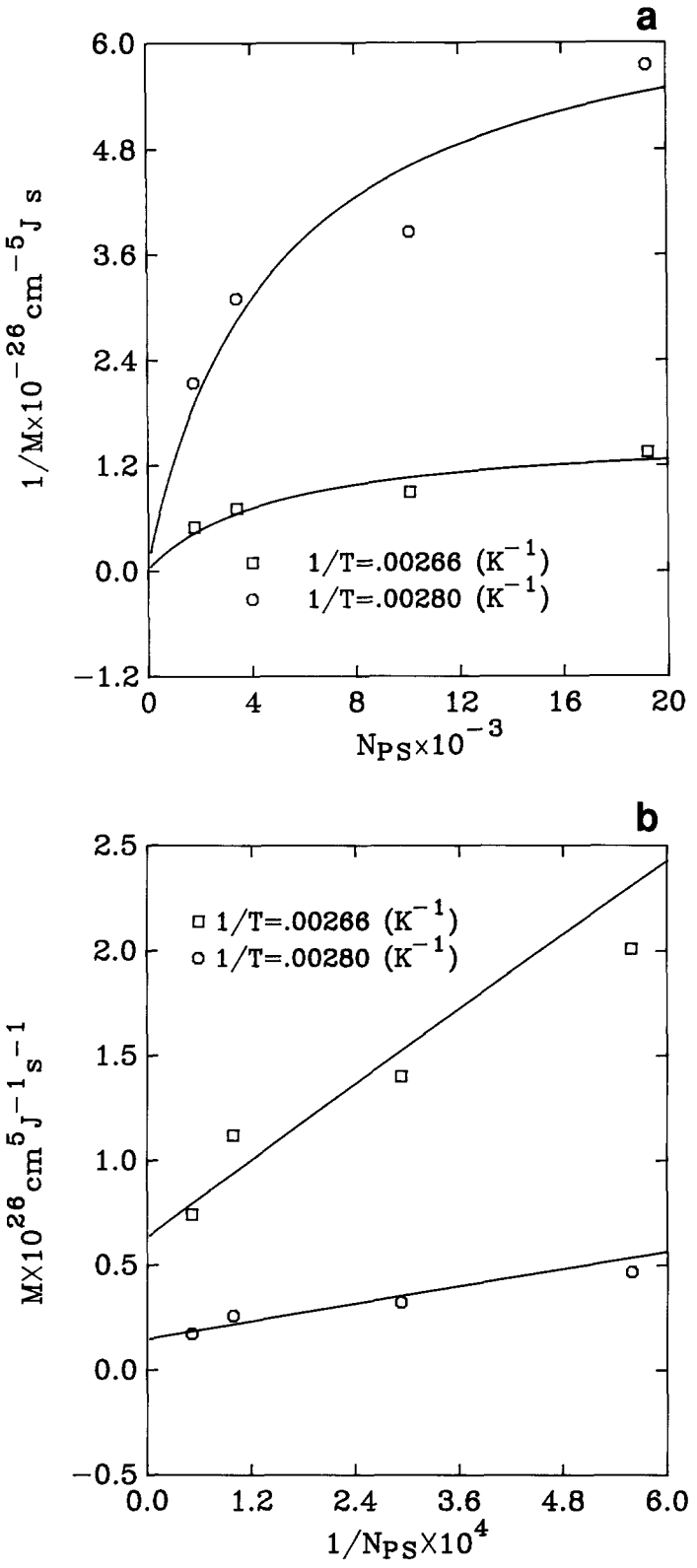

Figure 11 (a) Inverse mobility data, $1/M$, and (b) mobility data, M, of PS/PVME plotted against N_{PS} and $1/N_{PS}$, respectively, for the two temperatures indicated. Solid lines are calculated from the ANK equation (equation (17'))

the plot based on the fast mode theory tends to fail at large molecular weight of PB (*Figure 12a*) and that based on the slow mode theory tends to fail at smaller molecular weight of PB (*Figure 12b*). Both solid lines are calculated according to equations (10) and (17') with $\phi = 0.5$, $\bar{b}^2 = 0.42 \times 10^{-14}$ cm^2, $\alpha = D_1^{PB}/D_1^{SBR} = 1$, $X' = 1.0 \times 10^{-4}$ and $D_1^{SBR} = 6.6 \times 10^{-6}$ cm^2 s^{-1}. Also $v_A = v_B = v_0$ was used in this analysis. Similar to the PS/PVME case, the molecular weight dependence of mobilities can be nicely represented by the ANK equation. Again, for the SBR1/PI system, the same analysis has been carried out. M' *versus* $1/N_{PI}$ data are displayed in *Figure 13a* and

Table 5 D_{int} and $q_m(0)$ for the SBR10/PB blends and SBR1/PI blends in the early stage of spinodal decomposition

Sample	Temp. (°C)	$-D_{int} \times 10^{14}$ (cm^2 s^{-1})	$q_m(0) \times 10^{-4}$ (cm^{-1})
SBR10/PB5	70	36	9.0
SBR10/PB10	70	26.4	10.2
SBR10/PB20	70	17.9	9.1
SBR10/PB100	70	4.9	7.9
SBR1/P120	60	31.0	12.0
SBR1/PI55	60	13.0	9.5
SBR1/PI122	60	5.8	8.8
SBR1/PI273	60	2.8	8.4

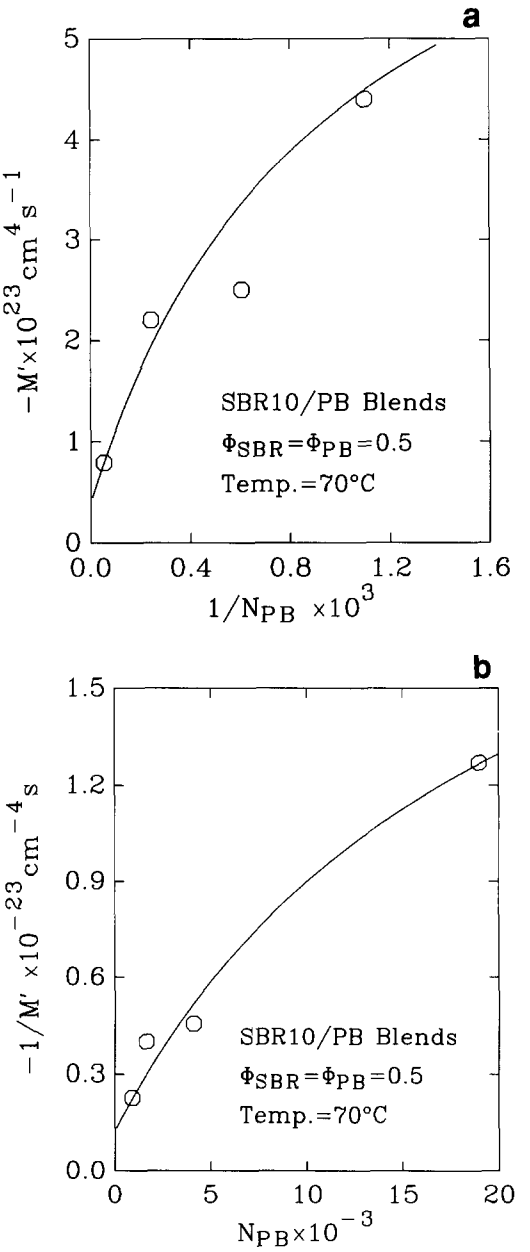

Figure 12 (a) Relative mobility data , M', and (b) inverse relative mobility data, $1/M'$, *versus* $1/N_{PB}$ and N_{PB}, respectively, for SBR/PB system. Solid line is calculated from the ANK equation (equation (17'))

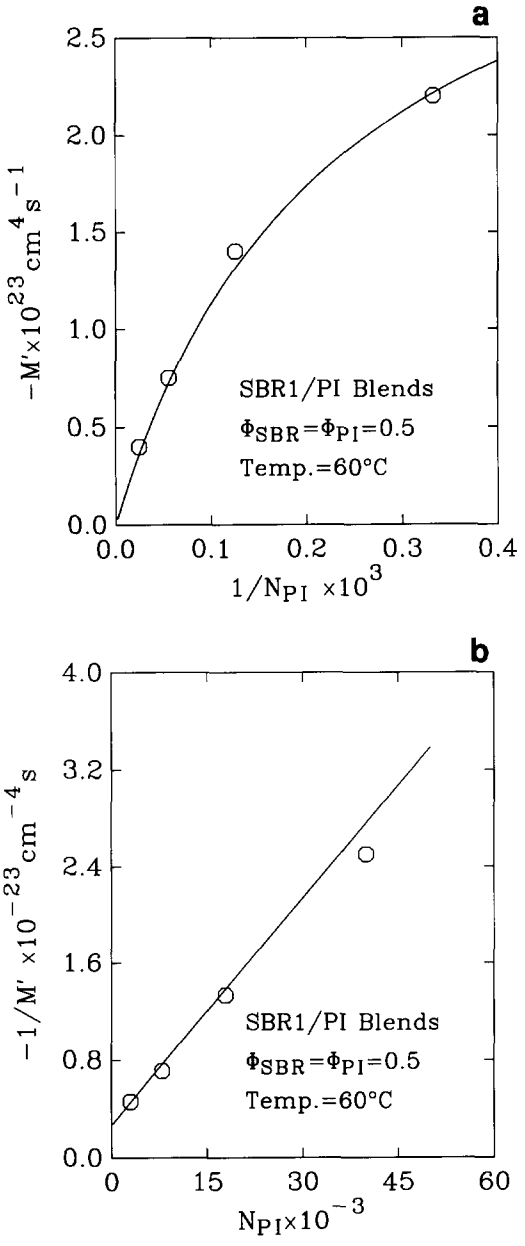

Figure 13 (a) Relative mobility data, M', and (b) inverse relative mobility data, $1/M'$, *versus* $1/N_{PI}$ and $1/N_{PI}$, respectively, for SBR/PI system. Solid line is calculated from the ANK equation

then replotted in *Figure 13b* as $1/M'$ *versus* N_{PI}. The experimental data (open circles) clearly support the slow mode in this case, as evidenced by linearity between $1/M'$ *versus* N_{PI} (*Figure 13b*) and by non-linearity between M' *versus* $1/N_{PI}$ (*Figure 13a*). This is because the lowest molecular weight of PI used in this study is much larger than the molecular weight of SBR1. The crossover to the fast mode is expected to be observed at a molecular weight of PI lower than that covered in this study, i.e. at the right-hand end of *Figure 13a* and the left-hand end of *Figure 13b*. The best solid line fitted with equation (17') is plotted as solid curves in *Figure 13a* and *b* with $\phi = 0.5, \bar{b}^2 = 0.49 \times 10^{-14}\,cm^2, \alpha = D_1^{PI}/D_1^{SBR} = 2.3$, $X' = 1.0 \times 10^{-5}$ and $D_1^{SBR} = 4.0 \times 10^{-6}\,cm^2\,s^{-1}$. Similarly to the PS/PVME and SBR10/PB cases, the molecular weight dependence of mobilities of the SBR/PI system can be nicely represented by the ANK equation. It should be noted, however, that X' for SBR1/PI is one order of magnitude smaller than X' for SBR10/PB, implying that slow mode is favoured for the SBR1/PI system. We do have to point out that the parameters used in all three systems may not be the only unique set which could fit the limited number of data points. Nevertheless, this ANK model seems to provide, at least qualitatively, a cross-over model from the vacancy picture to the incompressible picture and can reproduce experimental results fairly well. Still, a detailed molecular model for the dynamics has yet to be developed, and the uniqueness of the data analysis has to be studied.

We want to point out that this question of interdiffusion of a binary system is by no means completely understood from either a theoretical or from an experimental point of view. Experimental results are often inconclusive. This can possibly be said about this study as well. We took the most systematic study (to our knowledge) in the literature which is the study of PS/poly(xylenyl ether) (PXE) blends by Composto *et al.*[14] by means of forward recoil spectrometry. We analysed their results according to equations (13') and (14') and displayed them in *Figures 14a* and *b*. The D used in this notation is proportional to the mobility, M, used earlier in this paper. It is clear that the data can be represented by a straight line in both plots. If one does not invoke the estimated tracer diffusion coefficient of the polydispersed PXE component, then it will be difficult to judge which model is better. Moreover, if there is any deviation from the vacancy model by examining the molecular weight dependence of A, it will happen when $D_1^A/N_A \leqslant D_1^B/N_B$ or when N_A is large. This can be demonstrated by rearranging equation (17). If it is true that the second component gives a negligible contribution in this PS/PXE system, then equations (13') and (14') will become identical.

CONCLUSION

The mobility of PS/PVME blends has been studied as a function of temperature and PS molecular weight. This is carried out by measuring the time dependence of the static structure factor, $S(q, t)$, with a reverse quench from a temperature near the critical temperature to a temperature deeper in the miscible region. Since this experiment measures only the decay of the thermally induced concentration fluctuation from one equilibrium condition to another, the linearized diffusion equation can be used to extract the interdiffusion coefficient, D_{int}. Mobility M can then be obtained by dividing D_{int} by $\partial^2 \Delta f/\partial\phi_0^2$.

Similar studies have also been carried out for SBR/PB and SBR/PI systems. Homogenized specimens have been obtained by a uniaxial compression technique and then the early stage spinodal decomposition kinetics have been studied. Although a direct measure of $\partial^2 \Delta f/\partial^2\phi_0$ was not possible, the interdiffusion coefficient D_{int} and the relative mobility $M' = D_{int}/q_m^{2(0)} \sim M$ have been obtained.

It is clear from our results of all three systems that the mobility data can be represented nicely by the vacancy (fast mode) model in the lower molecular weight range but shows deviation at high molecular weights. Conversely, the same mobility data can be represented by the incompressible (slow mode) model at large molecular weights and deviates towards the vacancy model at low molecular weights. The recent calculation of Akcasu *et al.*[27] for a ternary system can be used to interpolate our

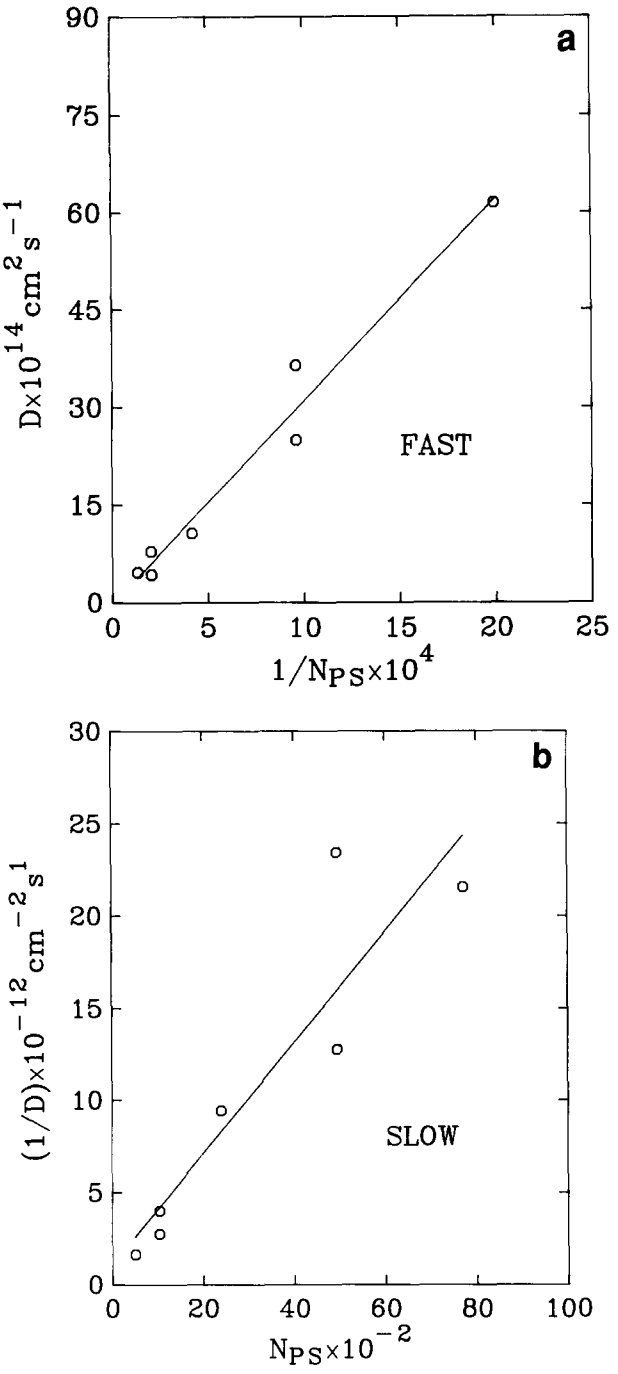

Figure 14 Data from reference 14 plotted as (a) D *versus* $1/N_{PS}$ and (b) $1/D$ *versus* N_{PS}

results very nicely. By treating the third component as vacancies, the ANK model can recover both vacancy model and incompressible model as limiting cases and is consistent with the results of this study. We should also point out that none of the three models mentioned above takes into account the coupling of diffusion coefficients[5] nor the dependence of monomeric frictional coefficient, ζ_1^i, of one component on the molecular weight of the second component. We believe that better theoretical calculation and experimental measurements are needed in order to have a better understanding of interdiffusion in a binary polymer system.

ACKNOWLEDGEMENT

The authors thank Professor A. Z. Akcasu for many stimulating discussions concerning polymer dynamics and interdiffusion.

REFERENCES

1 Brochard, F., Jouffroy, J. and Levinson, P. *Macromolecules* 1983, **16**, 1638
2 Binder, K. *J. Chem. Phys.* 1983, **79**, 6387
3 Schichtel, T. E. and Binder, K. *Macromolecules* 1987, **20**, 1671
4 Binder, K. *Colloid Polym. Sci.* 1987, **265**, 273
5 Jilge, W., Carmesin, I., Kremer, K. and Binder, K. *Macromolecules* 1990, **23**, 5001
6 Kramer, E. J., Green, P. and Palmstrom, C. J. *Polymer* 1984, **25**, 473
7 Sillescu, H. *Makromol. Chem., Rapid Commun.* 1984, **5**, 519
8 Sillescu, H. *Makromol. Chem., Rapid Commun.* 1987, **8**, 393
9 Foley, G. and Cohen, C. *J. Polym. Sci., Part B: Polym. Phys.* 1987, **25**, 2027
10 Murschall, U., Fischer, E. W., Herkt-Maetzky, Ch. and Fytas, G. *J. Polym. Sci., Polym. Lett. Edn.* 1986, **24**, 191
11 Brereton, M. G., Fischer, E. W., Fytas, G. and Murschall, U. *J. Chem. Phys.* 1987, **87**, 5048
12 Fytas, G. *Macromolecules* 1987, **20**, 1430
13 Composto, R. J., Mayer, J. W., Kramer, E. J. and White, D. *Phys. Rev. Lett.* 1986, **57**, 1312
14 Composto, R. J., Kramer, E. J. and White, D. M. *Nature* 1987, **328**, 234
15 Jordan, E. A., Ball, R. C., Donald, A. M., Fetters, L. J., Jones, R. A. L. and Klein, J. *Macromolecules* 1988, **21**, 235
16 Cahn, J. W. and Hilliard, J. E. *J. Chem. Phys.* 1958, **28**, 258
17 Cahn, J. W. *J. Chem. Phys.* 1965, **42**, 93
18 Cook, H. E. *Acta Metall.* 1970, **18**, 297
19 Sato, T. and Han, C. C. *J. Chem. Phys.* 1988, **88**, 2057
20 Hashimoto, T., Izumitani, T. and Takenaka, M. *Macromolecules* 1989, **22**, 2293
21 Izumitani, T. and Hashimoto, T. *J. Chem. Phys.* 1985, **83**, 3694
22 Takenaka, M., Izumitani, T. and Hashimoto, T. *Macromolecules* 1987, **20**, 2257
23 de Gennes, P. G. *J. Physique* 1970, **31**, 235
24 de Gennes, P. G. 'Scaling Concepts in Polymer Physics', Cornell University Press, Ithaca, 1979
25 Bauer, B. J., Hanly, B. and Muroga, Y. *Polym. Commun.* 1989, **30**, 19
26 Hamonda, B., Briber, R. and Bauer, B. personal communication, 1991
27 Akcasu, A. Z., Naegele, G. and Klein, R. *Macromolecules* 1991, **24**, 4408
28 Akcasu, A. Z. and Tombakoglu, M. *Macromolecules* 1990, **23**, 607
29 Akcasu, A. Z. *Macromolecules* 1991, **24**, 2109